Modeling the Steady Flow of Yield-Stress Fluids in Packed Beds

Matthew T. Balhoff and Karsten E. Thompson
Gordon A. and Mary Cain Dept. of Chemical Engineering,
Louisiana State University, Baton Rouge, LA 70803

DOI 10.1002/aic.10234
Published online in Wiley InterScience (www.interscience.wiley.com).

Network modeling has been performed to obtain quantitative and predictive results of the flow of yield-stress fluids in packed beds. Physically representative networks were used as the basis for the modeling, which have a one-to-one correspondence to computer-generated packed beds of spheres. The networks are able to account for the interconnectivity, heterogeneity, and converging/diverging geometry that are inherent in porous media. The approach can be used to model a wide range of non-Newtonian fluids, but the emphasis is for yield-stress fluids that can be represented using a Bingham model. For these fluids, a threshold pressure gradient is required to initiate flow, and flow at low pressure gradients is characterized by critical percolation behavior. Quantitative results of superficial velocity vs. pressure gradient are presented, and are compared to traditional bundle-of-tubes models, as well as limited experimental data available in the literature. Important differences are observed between the network model and the constitutive models. These are attributed mainly to heterogeneity and converging/diverging geometry, which are not accounted for in the semiempirical models. Comparison to experimental data is good for certain fluids. In other cases, the modeling suggests that effects other than fluid rheology may also have affected flow, such as adsorption or filtration. © 2004 American Institute of Chemical Engineers *AIChE J,* 50: 3034–3048, 2004
Keywords: Bingham fluids, porous media, polymer properties, computational fluid dynamics (CFD)

Introduction

Modeling flow in packed beds and porous media at the engineering scale usually employs semiempirical equations, such as the Ergun equation, Darcy's law, or the Carman-Kozeny equation. Implicit in these equations is a view of the porous medium as a continuum, meaning that velocity is a spatially averaged, superficial velocity. Accordingly, all the complexities of the microscopic pore structure are lumped into terms, such as permeability. These empirical approaches are backed by years of experimental validation, and are known to work well for single-phase flow of Newtonian fluids.

Correspondence concerning this article should be addressed to K. E. Thompson at karsten@che.lsu.edu.

While the Ergun equation accounts for nonlinearities caused by inertial forces, most other nonlinear behavior is difficult to account for in a general sense. Examples include multiphase flow and non-Newtonian flow. Multiphase behavior has been studied extensively because of applications, such as interfacial mass transfer in packed beds, multiphase flows in petroleum reservoirs, and groundwater flow under unsaturated conditions. Models of non-Newtonian behavior are not quite as well developed, but have still received significant attention because of applications, such as composite-materials processing (Skartsis et al., 1994), polymer processing and/or separations procedures (Satyadev et al., 2000), and petroleum recovery applications (Sorbie et al., 1989). The most common models for non-Newtonian flow in porous media have been derived from existing semiempirical theory. The simplest of these are bundle-of-tubes models or Carman-Kozeny-type models (Carman,

1939), which extend their Newtonian counterparts. However, these approaches require additional empirical parameters to be introduced, which makes the equations less general.

This article describes a first-principles (although approximate) model for the flow of non-Newtonian fluids through packed beds. Flow behavior predicted by the model is compared to existing empirical equations and limited experimental data. These comparisons have helped in interpreting empirical functionalities and answering certain questions (while raising others) regarding discrepancies in experimental vs. theoretical behavior.

Although the particular focus of this article is on Bingham fluids in packed beds, the model is general in two aspects. First, any number of constitutive equations can be used in the model, including the more general Hershel-Bulkley equation (Skelland, 1967), which exhibits both yield and power-law behavior. Second, flow is modeled using a network approach. Hence, while this discussion is for packed beds, it could equally well apply to natural unconsolidated media (Vogel and Roth, 2001), consolidated materials (Bakke and Oren, 1997), and fibrous materials (Thompson, 2002).

Ultimately, the role of the model described here is as a surrogate for a closed-form, continuum-scale equation: quantitative flow behavior is predicted as a function of measurable material and rheological properties. The advantage of this approach is the ability to account for any number of phenomena that are not reflected in traditional empirical equations, such as heterogeneity, interconnectivity, spatial correlations in physical properties, converging diverging flow geometries, critical behavior associated with percolation, and so on. With proper upscaling, the model can then be used (directly or indirectly) to generate superficial velocities for continuum-scale modeling of various engineering and materials-science applications.

Background

Non-Newtonian fluid models

Numerous constitutive equations have been proposed to describe the rheology of non-Newtonian fluids (Bird et al., 1987; Carreau et al., 1997), all of which account for shear-dependent viscosity in some way. Focusing on yield-stress fluids in particular, the constitutive equation must reflect the behavior that the material becomes fluid only after a critical shear stress is reached. The simplest yield-stress model is the Bingham model, in which the relationship between shear stress vs. shear rate is linear, with the yield stress defined as the *y*-axis intercept. A more general model is the Herschel-Bulkley Model, which includes the shear-thinning or shear-thickening behavior of power-law fluids and the yield-stress effect of the Bingham Model, as shown by Eq. 1

$$\tau_{xy} = \tau_0 + \mu_0 \left(\frac{\partial v_x}{\partial y} \right)^n \tag{1}$$

The Herschel-Bulkley model reduces to the ideal Bingham model for the special case where n is unity, and to the power-law model for no yield stress ($\tau_0 = 0$). Although more complex models may describe the rheology of specific fluids better, the Bingham and Herschel-Bulkley models are widely used due to their mathematical simplicity.

Macroscopic models for flow in porous materials

Several generalized equations have been developed for yield-stress fluids that are analogous to Darcy's law (which for isotropic permeability is $\boldsymbol{v} = (-K/\mu)\nabla P$). Park (1972) developed a modified Ergun equation for modeling one-dimensional (1-D) flow of a generalized Herschel-Bulkley fluid in a packed bed. Pascal (1981) proposed a modified Darcy's law for a Herschel-Bulkley fluid. He acknowledges a threshold gradient to initiate flow, but suggests that it must be determined experimentally. Using a bundle-of-tubes approach, Al-Fariss and Pinder (1985, 1987) were able to extend Pascal's model by deriving an equation for the threshold gradient. Vradis and Protopapas (1993) derived a 3-D form of Darcy's law for Bingham fluids. Chase and Dachavijit (2003) derived a modified Ergun equation, similar to the one presented by Park (1972), for the laminar flow of Bingham fluids in packed beds.

To gain insight into the semiempirical approach generally used in these derivations, we focus on the 1-D form of the modified Darcy's law presented by Al-Fariss and Pinder (1987). Approximating the porous medium as a bundle of capillary tubes, the following expression relates the superficial velocity and applied pressure gradient

$$v_0 = \left[\frac{-K}{\mu_{eff}} \left(\frac{\partial P}{\partial z} - \sqrt{\frac{C\phi}{2K}}\,\tau_0 \right) \right]^{1/n} \quad if \quad \frac{\partial P}{\partial z} > \sqrt{\frac{C\phi}{2K}}\,\tau_0 \tag{2}$$

where

$$\mu_{eff} = \left(\frac{\mu_0}{4} \right) \left(3 + \frac{1}{n} \right)^n (8C\phi K)^{(1-n)/2}$$

The earlier expression is applicable above the threshold pressure gradient required to initiate flow. The velocity is zero below the threshold. The equation shows that the threshold gradient is proportional to the yield stress, and is also a function of the porous medium morphology (through K). The constant C is an experimental tortuosity constant, the value of which varies in the range $\sqrt{2}$ to 25/12, depending on the source consulted. It should be noted that the modified Darcy law presented by Al-Fariss and Pinder (1987) incorporates an approximate velocity profile for flow so as to simplify the resulting expression. Physically, the approximation neglects the flat front of the velocity profile that occurs in unidirectional laminar flow of a yield-stress fluid, which would most affect calculations made at low flow rates (that is, when the applied pressure gradient is near the threshold pressure gradient).

The primary advantages of the modified Darcy's law shown in Eq. 2 are its simplicity and its similarity in form to Darcy's law. The other aforementioned macroscopic models were obtained using similar approaches, that is, from expressions for flow rate vs. pressure drop in a single capillary tube (see Table 1). Surprisingly, the models predict quite different results for the threshold gradient, as well as the velocity above the threshold gradient despite the fact that they are each derived in a similar way. Figure 1 compares the results for each of the models (without empirical adjustments) using hypothetical

Table 1. Equations for Flow Rate vs. Pressure Drop in a Cylindrical Capillary

Fluid Type	Equation for Flow Rate in Cylindrical Tube
Newtonian	$q = \frac{g}{\mu}\Delta P$
Power-Law	$q = \frac{g}{\mu_0^{1/n}}\left(\frac{4n}{3n+1}\right)\left(\frac{R}{2L}\right)^{(1/n)-1}\Delta P^{1/n}$
Bingham	$q = \frac{g}{\mu_0}\Delta P\left[1 - \frac{4}{3}\left(\frac{\tau_0}{\tau_w}\right) + \frac{1}{3}\left(\frac{\tau_0}{\tau_w}\right)^4\right]$
Herschel-Bulkley	$q = \frac{g}{\mu_0^{1/n}}\left[\frac{8L}{R}\frac{(\tau_w - \tau_0)^{1+(1/n)}}{\tau_w^3}\left(\frac{(\tau_w - \tau_0)^2}{3 + 1/n} + \frac{2\tau_0(\tau_w - \tau_0)}{2 + 1/n} + \frac{\tau_0^2}{1 + 1/n}\right)\right]$

$g = (\pi R^4/8L)$; $S = 2\pi RL$; $\tau_w = (\Delta PR/2L)$

rheological parameters $\tau_0 = 10$ Pa, $n = 1$, and, $\mu_0 = 0.1$ Pa-s, and porous medium parameters $D_p = 0.2$ cm and $\phi = 38\%$. The differences in predicted velocity would be even more significant for fluids that exhibit shear-thinning behavior in addition to a yield stress.

It is generally recognized that these semiempirical approaches require matching to experimental data to correct for the limitations built into the models. With the limited amount of data that are available, it is not yet clear whether universally applicable adjustments can be made (as with the Ergun equation for Newtonian flow), or whether a case-by-case assessment is needed, in which case the empiricism is less useful. Qualitative arguments reveal limitations in the bundle of tubes models that may be less consequential for Newtonian flow, but that are important for predicting yield-stress behavior. First, the distribution of pore sizes in a real material produces a critical percolation effect for yield-stress fluids (Sahimi, 1993; Shah et al., 1995) that does not occur in a uniform bundle of tubes. Second, we show later that the converging-diverging behavior of individual throats has a prominent effect for yield-stress fluids.

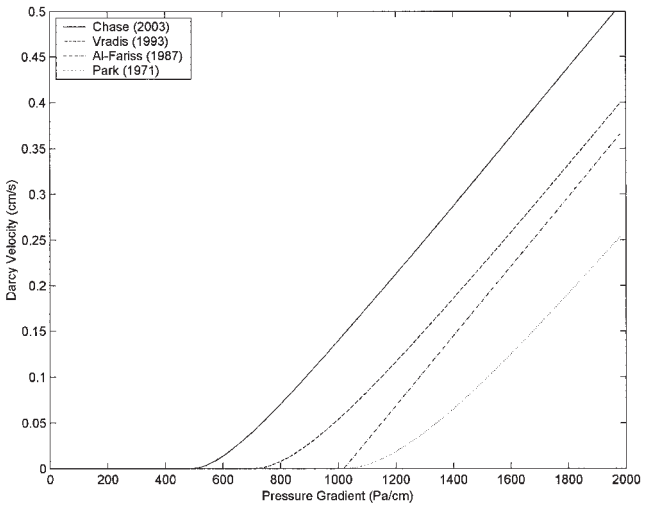

Figure 1. Darcy velocity vs. pressure gradient as modeled by various bundle-of-tubes models.

For the purpose of comparison, bed and rheological properties were chosen as $D_p = 0.2$ cm, $\phi = 38\%$, $\tau_o = 10$ Pa, $\mu_o = 0.1$ Pa-s. (Permeability was computed using Blake-Kozeny equation (Bird et al., 2002) to be 3.81×10^{-5} cm^2.)

Experimental work

A limited amount of experimental work has been published for the flow of yield-stress fluids in packed beds. Park (1972) measured friction factor as a function of modified Reynold's number using solutions of polymethylcellulose, which is modeled in his work as a Herschel-Bulkley fluid. The data were compared to the theoretical friction factor obtained from the modified Ergun equation. Although excellent agreement between experimental and theoretical friction factor is presented in his dissertation, we were unable to reproduce these results using their tabulated data. Al-Fariss and Pinder (1985, 1988) measured pressure gradient vs. Darcy velocity in a packed bed using paraffinic wax in oil, and compared the data to the modified Darcy law (Eq. 2). Chase and Dachavijit (2003) obtained similar data for various concentrations of Carbopol solution (approximately a Bingham fluid), and compared the data to their modified Ergun equation. Recognizing the limitations of the macroscopic models, Al-Fariss and Pinder (1987), as well as Chase and Dachavijit (2003), treated constants in the empirical models as adjustable parameters to better match the models to their data. Al-Fariss and Pinder (1987) adjusted the threshold gradient, power-law index n, and permeability K, to fit the data. Since permeability was measured independently from Newtonian tests, their approach is analogous to introducing a relative permeability term that accounts for the non-Newtonian behavior. They perform adjustments on a case-by-case basis, and no universal methodology is proposed. Chase and Dachavijit (2003) added a single experimental constant in the threshold gradient term, which was assigned a universal value so as to best fit all of their experimental data. The correction is attributed to inaccuracies in the bundle-of-tubes approximation.

Network modeling

Network modeling is a pore-scale technique in which a porous medium is approximated as an interconnected network of pores and pore throats. It makes use of first-principles equations in the model formulation, making it ideal for situations where empiricism is not effective. At the same time, approximations to the fluid mechanics and the pore morphol-

ogy allows modeling to be performed over orders-of-magnitude larger characteristic length scales than numerical techniques where the equations of motion are solved directly.

Network modeling has been used to study a large number of phenomena, including permeability (Bryant et al., 1993), solute dispersion (Sahimi and Imdakm, 1988), multiphase flow (Lenormand et al., 1988), contaminant transport (Dillard and Blunt, 2000), inertial flows (Thauvin and Mohanty, 1998), and more. In the past, much of the modeling has been performed on idealized networks, in which case the results are largely qualitative. During the past 10 years, however, new techniques for network generation and flow modeling have been developed that allow them to be used in a predictive sense for certain applications.

Most network modeling studies of non-Newtonian flow deal with shear-thinning fluids (that have no yield stress). Sorbie and Clifford (1989) modeled the flow of a Carreau fluid using 2-D networks. Quantitative parameters were defined (for example, permeability, area) and used to investigate macroscopic flow rate vs. pressure drop. However, comparison to real porous media is difficult because the networks are 2-D. Shah and Yortsos (1995) used 2-D and 3-D networks to model the flow of power-law fluids in porous media. They present qualitative results for the steady flow, which show that flow patterns are more sensitive to the throat-size distribution than for the case of Newtonian fluids. Shah et al. (1998) used similar networks to study displacement patterns involving power-law fluids. Recently, Lopez et al. (2003) used physically representative networks to model shear-thinning fluids in both consolidated and unconsolidated porous media, and showed good agreement with existing experimental data.

Modeling the flow of yield-stress fluids presents an additional challenge, because a finite pressure gradient is required to initiate flow in a throat. This effect can cause numerical difficulties because the pressure distribution is indeterminate in regions where the flow has not yet yielded. Sahimi (1993) modeled general nonlinear behavior in square (2-D) and cubic (3-D) networks, which included modeling piecewise linear transport within a network that contained thresholds for bond conductivities. This approach serves as an approximation for yield-stress flow through porous media (among other applications given). An equation analogous to Bingham flow in a capillary (although somewhat simpler) is used for flow in a throat. Although the network contained a distribution of threshold potentials, each bond was given the same value of conductivity. Consequently, emphasis was placed on determining the critical gradient required to initiate transport in the network. In real situations, the flow behavior above the critical gradient will depend on the distribution of conductivities in the network in addition to the threshold values. Shah et al. (1995) modeled the flow of a Bingham fluid in 2-D networks. Percolation patterns in the network are presented at various values of dimensionless yield stress. Images of the simulations illustrate that the number of percolating pathways for flow decreases as the dimensionless yield stress (σ_o) increases. Furthermore, a dimensionless critical yield stress (σ_{oc}) is identified for the network, which denotes the applied pressure gradient required for a percolation path to form. It is shown that σ_{oc} depends on the heterogeneity and interconnectivity in the network. Additionally, qualitative results are presented of a Bingham fluid displaced by a Newtonian fluid.

Objectives of the current work

In this work, the flow of non-Newtonian fluids in a packed bed is modeled using a first-principles approach. For simplicity, we present results for Bingham fluids, but the numerical model is being run with a variety of nonlinear constitutive equations.

Computer-generated sphere packings are used as models of packed beds, and are mapped onto networks of interconnected pores and throats. Flow modeling is used to predict macroscopic velocity as a function of applied pressure gradient. The key difference between this approach and the semiempirical approaches described earlier is that this model explicitly accounts for fluid rheology and pore structure without adjustable parameters. The difference between the current model and previous network models is the ability to perform quantitative, predictive modeling, based on measurable input parameters (that is, fluid rheology, particle size, and particle-size distribution).

Modeling Approach

Model of the packed bed

The packed beds used in the model are computer-generated random sphere packings. They are created using a collective rearrangement algorithm, which is one of two common methods for computer simulations of sphere packings, the other being sequential addition algorithms (Powell, 1980). The latter type of algorithm operates by the sequential addition of spheres to the edge of an existing bed or agglomerate. The main advantage to this approach is the ability to ensure point contacts between neighboring particles, which in turn leads to gravitationally stable packings. However, this approach has a number of drawbacks, the foremost being the inability to control porosity effectively.

Collective rearrangement algorithms are initiated by placing spheres randomly (or with a random component) into a prescribed domain without regard to whether sphere overlaps occur. For porosities of practical interest, overlaps are inevitable, but are then removed by iterative rearrangement of the sphere positions. In its simplest form, collective rearrangement consists of small, random movements of spheres in the packing; a move is accepted if it reduces the amount of overlap and is otherwise rejected. More elaborate strategies have been devised to improve the convergence speed, which typically add a logical component to the random displacements (for example, Jodrey and Tory, 1985).

The advantages of this approach include the ability to incorporate spatial correlations into the packing, and to prescribe the porosity of the packing *a priori*. (Assuming that all overlaps will eventually be removed, porosity is determined as soon as the domain size is specified and a given volume of spheres is placed into it.) The two drawbacks to this approach are that it is relatively slow, and that it does not ensure point contacts between spheres. This latter point, in theory, precludes the construction of gravitationally stable packings. However, in the porosity ranges that are physically representative of packed beds (36 to 40% for monodisperse sphere size), the resulting particle-particle gaps are insignificant compared to particle diameters, and do not influence the modeling of viscous flows.

The collective rearrangement algorithm used in this work

Table 2. Geometric Parameters Defining the Network Structure

Variable Association	Variable Name	Variable Type	Dimension
Network	Domain dimensions	vector	length
Pore	Location	vector	length
	Void volume	scalar	length^3
	Maximum inscribed radius	scalar	length
Throat	Interconnectivity:periodicity	scalar:vector	
	Cross-sectional area	scalar	length^2
	Maximum inscribed radius	scalar	length
	Surface area	scalar	length^2
	Hydraulic conductivity	scalar	length^3

imposes fully-periodic boundaries on the computational domain to eliminate edge effects in the packing. Sphere radii are selected randomly from a prespecified distribution (which can be of arbitrary form). If necessary, spatial correlations in sphere size can be incorporated using geostatistical kreiging techniques (Jensen et al., 1997). For a given distribution of sphere sizes, two of the following three parameters can be specified independently: number of spheres, domain size, or porosity. The remaining parameter then depends on the other two selections.

Network structure

Specification of the position and radius of each sphere in the packing is sufficient to completely define the structure of the void space in which fluid is transported. However, it is a continuous, interconnected region with a complex geometry. Hence, some form of discretization is required prior to numerical simulation. In the network-modeling approach, the continuum void space is discretized into pores and pore throats. The challenge is to obtain a network structure that effectively represents the true pore-space morphology.

In this work, networks are generated using a modified Delaunay tessellation (MDT) algorithm (Al-Raoush et al., 2003), which consists of three key steps:

(1) Perform a periodic Delaunay tessellation using the sphere centers. This step organizes the pore space into a collection of space filling tetrahedrons, each having a sphere centered at its four vertexes. This approach has been used in the past for characterizing random packings because of the natural correspondence of tetrahedrons to pores and the faces of tetrahedrons to pore throats (Mellor, 1989).

(2) Using the Delaunay cells as seed points, perform numerical optimization to find the largest spheres that can be inscribed into local voids in the packing. In cases where a single void is composed of multiple Delaunay tetrahedrons, merge these tetrahedrons into a single polyhedron. As with the original tetrahedrons, the tightest pore-to-pore constrictions are necessarily projected onto the faces of the polyhedrons, thus defining the pore throats.

(3) Perform a detailed geometric analysis of each pore to calculate critical parameters for modeling fluid transport. These parameters may include (but are not limited to) those listed in Table 2.

The MDT algorithm has a number of important features. First, the procedure described in step 2 is a rigorous analysis to locate local void spaces in the packing. Second, the process allows the interconnectivity between pores to be defined naturally, with no geometric restrictions on the pore coordination number. Third, the network is physically representative, meaning that a one-to-one correspondence exists between the network and the original packing, and no morphologic information is lost in constructing the network. Finally, the parameters used to describe the network (Table 2) are rigorous geometric parameters (except hydraulic conductivity, which is a dynamic parameter). Hence, the morphology of the original packing is not compromised by defining the network structure.

The implications of the third and fourth points are significant, mostly because the network is not transformed into a network of capillary tubes (a process that does compromise the morphologic description). Note in Table 2 that no capillary radius or length is listed. (The throat radius is a physical dimension measurable from the packing: the inscribed radius at the tightest constriction of each throat.) An additional benefit of generating a physically representative network is that, because of the one-to-one correspondence of the network to the original packing, additional morphologic parameters can be extracted if necessary.

Determining the parameters listed in Table 2 is not trivial. The process is described in more detail in Al-Raoush et al. (2003), but is summarized here for completeness. Domain dimensions are specified from the original sphere packing. The location of each pore is the location of each maximum-radius inscribed sphere found within the packing (inscribed spheres with significant overlap are merged). The void volume of each pore and the cross-sectional area of each throat can be calculated analytically for cases where sphere overlaps are negligible. The radii of inscribed spheres (pores) and circles (throats) are found by numerical optimization routines. The hydraulic conductivity can be calculated using a variety of approaches. In this work, we use a combination of the techniques described by Bryant et al. (1993) and Thompson and Fogler (1997), which gives reasonable quantitative results. Work is currently underway to assess the validity of these calculations via comparison to CFD results. Finally, the surface area of each throat is obtained by assigning a fraction of each sphere surface to the appropriate throat that it bounds. Figure 2 illustrates the transformation of the random sphere packing into a discrete network of pores and throats.

Modeling fluid flow in the network

The general approach to network modeling is to impose a mass conservation equation at each pore in the network. For

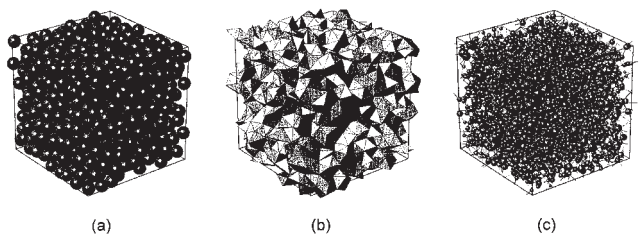

Figure 2. Transformation of a random packing into a physically representative network.

(a) 1,000-sphere periodic random packing; (b) 3-D periodic Delaunay tessellation; (c) 3-D periodic network generated using the tetrahedron-merging algorithm.

constant-density fluids, the conservation equation for pore i is simply

$$\sum_j q_{ij} = 0 \tag{3}$$

where q_{ij} is the volumetric flow rate into pore i through a throat connected to neighbor j. The flow rate q_{ij} is then written in terms of unknown pore pressures, which become the dependent variables in the problem. Hence, an expression for flow rate as a function of pressure drop in each throat is needed for substitution into Eq. 3. For low Reynolds-number flow of Newtonian fluids, flow rate is linearly proportional to the pressure drop, and substitution of a general expression for flow rate gives

$$\sum_j \frac{g_{ij}}{\mu}(P_j - P_i) = 0 \tag{4}$$

where g_{ij} is the hydraulic conductivity of the pore throat connecting pores i and j, μ is the fluid viscosity, and P represents point values for pore pressure.

In this work, network simulations are run at specified pressure gradients, so that the boundary conditions for the network consist of fixed inlet and outlet pressures. For a network of N pores, Eq. 4 is written once for each pore in the network to give a system of N equations for N unknown pore pressures. For throats that connect a pore to the inlet or outlet, P_j is known and the term $(g_{ij}/\mu)P_j$ contributes to the righthand side of the matrix equation. (Alternatively, to run simulations at constant flow rate, an additional equation is imposed forcing the sum of all inlet flow rates to equal the specified total volumetric flow rate. An additional unknown is also generated in this process, usually the inlet pressure.)

For non-Newtonian fluids, expressions for q_{ij} are not available, except for specific geometries, such as cylindrical ducts. However, to efficiently model flow in the network, analytical expressions for q_{ij} (even if approximate) are needed for substitution into Eq. 3. Three possibilities have been considered to address this problem: (1) Use Table 1 equations directly by assigning an equivalent radius and length to each throat; (2) create new equations for flow, based on the representative throat geometry, while maintaining the basic functionality of the capillary tube equations; (3) perform CFD on the relevant geometries to generate empirical expressions for flow. Regardless of the technique employed, the equations for q_{ij} will be nonlinear in pressure. Accordingly, a set of simultaneous nonlinear algebraic equations must be solved to determine the pressure field in the network.

Modeling flow in a single throat

Although the third option for obtaining q_{ij} is the most rigorous (that is, empiricism based on CFD simulations), it is difficult to justify given other simplifying assumptions that are inherent to the network approach. Furthermore, although detailed finite element simulations are presented later, using CFD to directly estimate throat conductivities has obvious practical drawbacks. First, the real throats are not axisymmetric, and, thus, would require full 3-D simulations. Second, rigorous simulation on a throat-by-throat basis is not possible, because of unknown boundary conditions. Third, there is no assurance that the resulting correlations for q_{ij} could be generalized to all packing structures, which may require new CFD simulations to be performed each time conditions are changed. Finally, the correlation would be entirely empirical, making phenomenological interpretation of behavior more difficult.

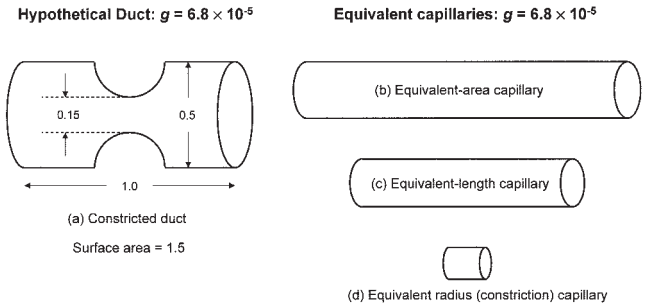

Figure 3. Hypothetical duct to various capillaries with equal conductivity.

(a) hypothetical converging/diverging duct: $g = 6.8 \times 10^{-5}$, $S = 1.50$; (b) equivalent-surface-area capillary: $R = 0.133$, $L = 1.80$; (c) equivalent-length capillary: $R = 0.115$, $L = 1.0$; (d) equivalent-constriction capillary ($R = 0.075$, $L = 0.182$).

The first option (transformation of the network into capillaries) is certainly desirable because of its simplicity. However, it introduces ambiguity to the model, as illustrated by the following arguments. If the converging/diverging throats from the real packing are transformed into capillary tubes, the capillaries must be constructed in such a way that flow rate would be the same as in the corresponding duct for a given applied pressure drop. Considering the simple case of creeping Newtonian flow, this transformation (although unnecessary if g is presumed to be known) simply requires defining a capillary that has an equal hydraulic conductivity as the actual throat. Since a capillary geometry has two degrees of freedom (for example, radius and length), an infinite number of choices would be viable for creeping Newtonian flow.

For non-Newtonian flow, the relationship between flow rate and pressure drop is more complex. The conductivity alone cannot be used to predict flow, even in a capillary (see Table 1). Hence, transforming the real throats into equivalent capillary tubes requires enforcing a second geometric constraint. The ambiguity arises because several options exist for this second constraint (see Table 2), including the constriction radius, pore-to-pore length, and surface area, meaning that no single capillary network can uniquely represent the true packed bed.

The point can be illustrated rather dramatically using Figure 3, which shows a hypothetical converging/diverging duct, along with three transformed capillaries, each with the same conductivity as the duct, but with different properties imposed as the second constraint. For the current work, we require equivalent capillaries in which flow commences at the correct critical pressure drop (in addition to predicting the correct flow rate at high-pressure drops). Since shear stress acts over the inner surface area of the duct, the Figure 3b duct might appear to be the most appropriate approximation, because it has equal interior area S, and equal conductivity g to the constricted duct. However, numerical simulations show that this is not the case, as illustrated by Figure 4 (see Appendix A also), which compares flow through the hypothetical duct vs. flow through the

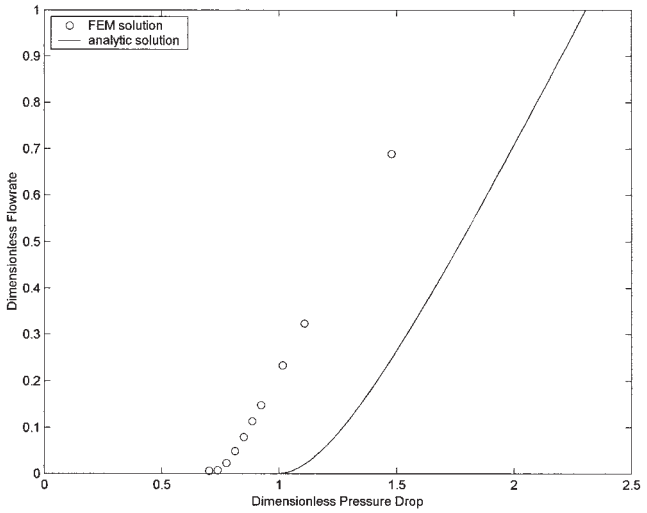

Figure 4. Bingham flow in a hypothetical duct (Figure 3a) vs. flow in the equivalent-surface-area capillary (Figure 3b).

Dimensionless pressure drop is defined as the pressure drop divided by the critical pressure drop required to initiate flow in a capillary. The dimensionless flow rate is defined as the flow rate divided by the flow rate of a Newtonian fluid with viscosity μ_0 at dimensionless pressure drop of 1.

equivalent-area capillary. The reasons for the discrepancy are related to the geometry of the true capillary. Since the inner surface is everywhere tangent to the velocity, shear stresses in the fluid are distributed evenly over the tube's interior surface. Thus, when the fluid first yields, it yields everywhere at the wall, allowing the Bingham material to move as a solid body (except exactly at the wall). In contrast, for the converging/diverging duct, the wall is not tangent to the shear stress everywhere and stress is not uniformly distributed over the inner surface. Consequently, as stress is applied to the converging/diverging duct, confined pockets of the material can yield well before bulk flow occurs. This behavior is illustrated by Figure 5, which shows the stress distribution in a Bingham fluid as increasingly large pressures are applied to one side of the axisymmetric duct. The contour lines represent the yield stress of the fluid for this particular case, and, thus, separate regions of yielded vs. unyielded material.

The advantages of the capillary-tube equations from Table 1 are their simplicity and that they are based on fundamentals. A compromise method that retains these attributes is the second possibility listed in the previous section: to use the functionality of the capillary equations, but to empirically adjust key parameters to more accurately simulate the fluid dynamics in the true pore throats of the packing. Adjustments can be made specifically for each individual fluid type; therefore, a set of equations analogous to those in Table 1 would be applicable for the network. The details of this approach for the specific case of a Bingham fluid are as follows.

Following Table 1, the equation for flow rate of a Bingham fluid through an arbitrary geometry is assumed to have the form

$$q = -a_0 \frac{\tau_0}{\mu_0} + a_1 \frac{1}{\mu_0} \Delta P + a_2 \frac{\tau_0^4}{\mu_0} \frac{1}{\Delta P^3} \tag{5}$$

where the constants a_0, a_1, and a_2, are geometric parameters for the duct. For a capillary tube, these constants can be written in terms of the radius and length (see Table 1)

$$a_{0,cap} = \frac{\pi R^3}{3} \quad a_{1,cap} = \frac{\pi R^4}{8L} \quad a_{2,cap} = \frac{2\pi L}{3} \tag{6}$$

The constants could also be written in terms of the conductivity (g) and surface area (S) of the capillary. This format is more useful since both of these parameters are known for the actual throats, as shown in Table 2

$$a_{0,cap} = \frac{\pi}{3}\left(\frac{4Sg}{\pi^2}\right)^{3/5} \quad a_{1,cap} = g \quad a_{2,cap} = \frac{\pi}{3}\left(\frac{S^4}{128\pi^3 g}\right)^{3/5} \tag{7}$$

For the general case of a converging/diverging duct, the constants are assumed to be some function of the known geometric properties

$$a_0 = f_0(g, S, \gamma_R) \quad a_1 = f_1(g, S, \gamma_R) \quad a_2 = f_2(g, S, \gamma_R), \tag{8}$$

where we have assumed that the aspect ratio of the constriction is a third key parameter.

Equation 7 cannot be substituted directly for Eq. 8, because of the problem illustrated by Figure 4. However, we argue that the functionality of Eq. 7 can remain intact, with small empirical adjustments. In fact a_1 must equal g for any shaped duct, because as ΔP approaches infinity, the fluid is approximately Newtonian. In such a case, Eq. 5 must reduce to the Newtonian equation for flow, and a_1 would equal the conductivity. Since substitution of the total duct surface area into Eq. 7 would overpredict the yield point (pressure drop required to initiate flow), adjustments must be made to those terms that include the duct surface area.

To determine the coefficients for the duct (Eq. 8), an effective surface area is defined so that the analytic expression for flow rate (Eqs. 5 and 7) can still be used. This effective area is calculated, based on the error in the critical pressure drop for

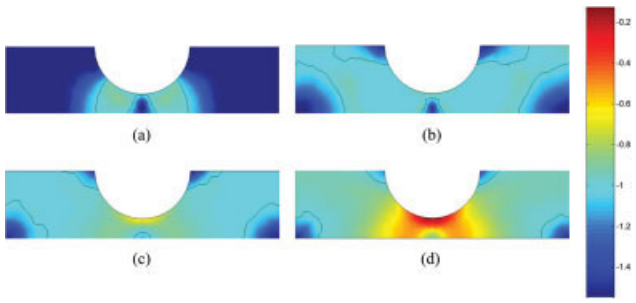

Figure 5. Images of stress distributions in converging/diverging ducts at increasing pressure drops: (a) $\Delta P_D = 0.5$; (b) $\Delta P_D = 0.78$; (c) $\Delta P_D = 1.0$; (d) $\Delta P_D = 2.0$.

Color corresponds to a log representation of the second invariant of the stress tensor: $\sqrt{(1/2)\boldsymbol{\tau} : \boldsymbol{\tau}}$.

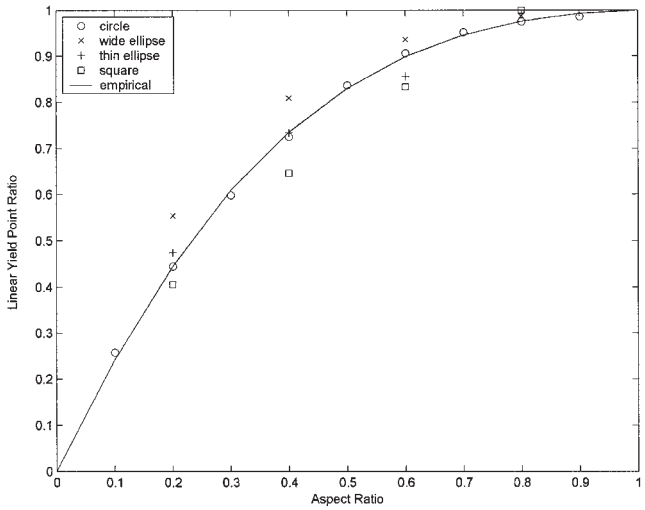

Figure 6. Linear yield point ratio vs. aspect ratio for various duct types.

Equation represents best fit to ducts with constrictions of constant curvature.

flow (ΔP^*), defined by the yield-point ratio (YPR): the ratio of the critical pressure drop for the duct to the critical pressure drop for the equivalent-area capillary tube. Essentially equivalent, but more convenient for numerical computation, is the linear yield-point ratio

$$\text{LYPR} = \left(\frac{\Delta P^*_{lin,duct}}{\Delta P^*_{lin,cap}}\right) \tag{9}$$

where the linear yield points are found by extrapolating the linear portions of the curves from Figure 4 ($\Delta P \gg \Delta P^*$) back to the x axis.

Values of LYPR were obtained by running finite-element simulations of Bingham flow for a large number of duct geometries (see Appendix A). From these data, a strong correlation was found between LYPR and the aspect ratio γ_R of the ducts (which in the network we define as the ratio of the inscribed constriction radius to the inscribed pore radius). The correlation is shown in Figure 6; the different symbols represent different types of constrictions. The circles are constrictions of constant curvature. These are the most similar to constrictions in the network model, which are formed by spheres. Hence, these data were used to formulate the empirical equation

$$\text{LYPR} = \frac{0.261\gamma_R}{1 + 0.686\gamma_R + 0.929\gamma_R^2} \tag{10}$$

Given the network parameters from Table 2, the aspect ratio of a throat can be approximated as the ratio of inscribed throat radii to pore radii, and LYPR is obtained using Eq. 10. Once an estimate of LYPR is obtained for a specific duct geometry, it must be translated into an effective surface area S_{eff}, as follows. Combining Eqs 5 and 7, setting the flow rate equal to zero, and retaining only the linear terms gives

$$q = 0 = \frac{g}{\mu_0}\Delta P - \frac{\pi}{3}\left(\frac{4Sg}{\pi^2}\right)^{3/5} \tag{11}$$

Equation 11 can be rewritten in terms of the linear critical pressure drop

$$\left(\frac{16\pi g^2}{S^3}\right)^{1/5}\Delta P^*_{lin,cap} = \frac{4}{3}\tau_0 \tag{12}$$

which is applicable for a capillary tube. The equivalent equation for a generalized duct is

$$\left(\frac{16\pi g^2}{S^3_{eff}}\right)^{1/5}\Delta P^*_{lin,duct} = \frac{4}{3}\tau_0 \tag{13}$$

Dividing Eq.12 by Eq 13 provides an expression relating the effective surface area to the linear yield point ratio

$$\text{LYPR} = \frac{\Delta P^*_{lin,duct}}{\Delta P^*_{lin,cap}} = \left(\frac{S_{eff}}{S}\right)^{3/5} \tag{14}$$

In the network model, S_{eff} is obtained from Eqs. 10 and 14. S_{eff} is then used in place of S in Eq. 7, thus, generating coefficients for a semi-analytic expression for q_{duct} as a function of the pressure drop, rheological properties, and geometric properties.

Figure 7 shows agreement between the semi-analytical expressions and numerical simulations for Figure 3a duct. The comparison shows good agreement except at low-pressure drops. The error in this range is essentially because the constant a_0 in Eq. 6 was adjusted to account for the converging/diverging geometry, but a_2 was not. However, because the error is at low flow rates, it is relatively less important and further refinement is probably not justified given that the empiricism is based on idealized converging-diverging ducts with simple boundary conditions.

Numerical solution

Figure 8 illustrates the relationship between dimensionless flow rate and dimensionless pressure drop in a capillary (or converging/diverging duct; the functionality is assumed to be the same in this model). The shapes of these curves are indicative of the types of nonlinearities that must be dealt with in the numerical solution. For the case of power-law fluids, direct solution of the nonlinear equations using the multidimensional Newton-Raphson method has proved convergent and highly efficient in all cases tested. However, solution of the Bingham or Herschel-Bulkley flow equations is less stable due to the zero-flow region that appears for any yield-stress fluid (that is, before the wall stress is sufficient to overcome the yield stress).

To address these convergence problems, a modified Bingham (or Hershel-Bulkley) equation is used, which approximates the true functionality but allows a finite flow rate to occur at all pressure drops. Because the modified curve has a finite slope below the critical pressure drop, it lends stability to the numerical algorithm. The modified equation is derived by assuming power-law behavior between zero and ΔP_m, which is an arbitrarily selected pressure drop that is greater than the dimensionless pressure drop required to initiate flow. In fitting

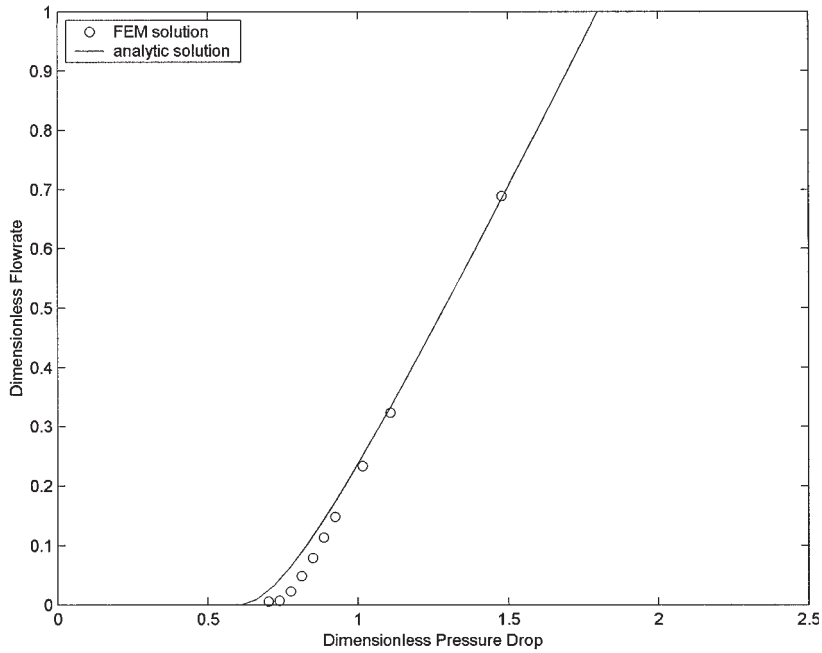

Figure 7. Bingham flow in a hypothetical duct (Figure 3a) to the analytical solution in the empirically defined equivalent capillary.

the modified equation, two unknown parameters arise, which are determined by forcing continuity in the value and its first derivative where the modified curve meets the true Bingham equation (at ΔP_m). Figure 9 illustrates the shape of modified curves for matching points of $\Delta P_m = 3.0$, 2.0, and 1.5 times the critical pressure drop.

To achieve a rigorous solution for flow of a yield stress fluid, the problem is first solved using the modified Bingham equation with $\Delta P_m = 20$, which leads to universal convergence for the cases we have tested. ΔP_m is then lowered incrementally to a value near ΔP^* (for example, 1.01 ΔP^*), with the pressure field from the previous solution used at each subsequent step down. When the matching point is reduced to some small value, the resulting pressure field is then used as an initial guess for the true Bingham constitutive equation.

Once a solution for the pressure field in the network is

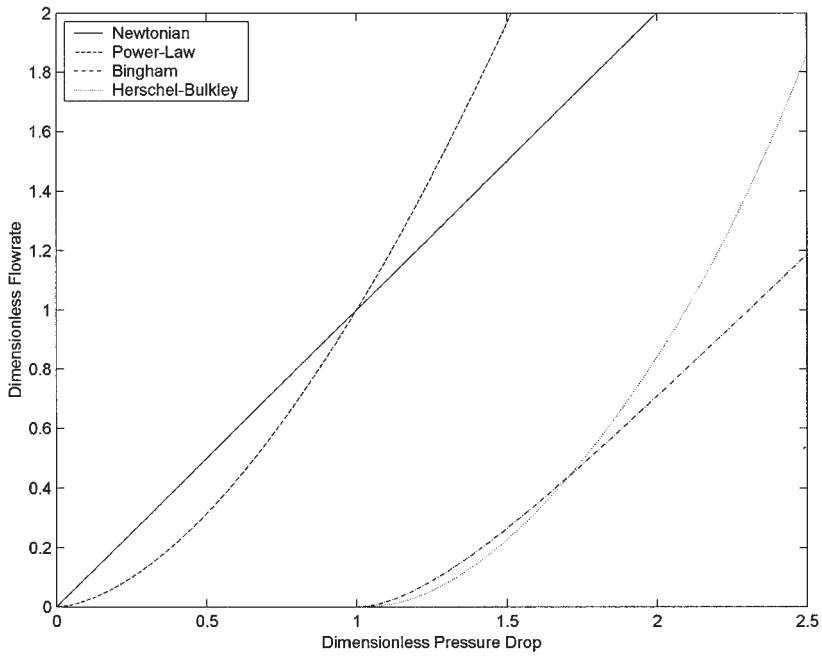

Figure 8. Dimensionless flow rate vs. pressure drop in a capillary tube for various rheological models.

Equations can be found in Table 1.

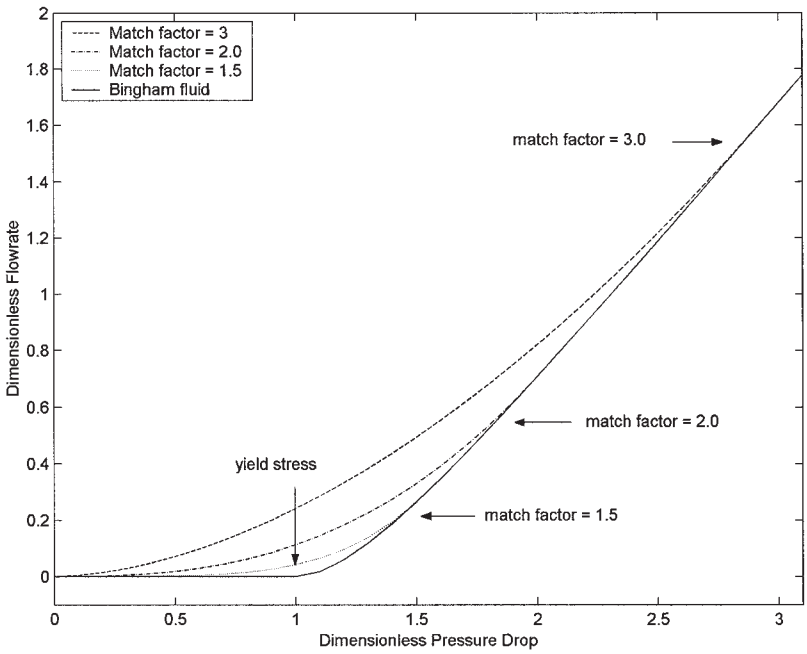

Figure 9. Exact and approximate solutions for dimensionless flow rate versus dimensionless pressure drop.

Approximate solutions used during iterations to increase numerical stability.

known, it can then be used to calculate various flow properties, the most important of which is the Darcy velocity (because it is the parameter of interest for modeling at the macroscopic scale). Certain results presented below are shown as plots of Darcy velocity vs. applied pressure gradient. Each of these plots can be viewed as a numerical replacement for Darcy's law for that particular fluid and porous material.

Results and Discussion

Qualitative behavior

In a single pore throat, flow commences only when sufficient internal stress exists such that the yielded material becomes uncontained, as described in the discussion of Figure 5. The specific behavior is a function of the throat size, geometry, and pressure drop across the throat. For a capillary tube, the behavior is particularly simple, with flow occurring when the wall stress $\tau_w = \Delta P(R/2L)$ exceeds the yield stress.

For an interconnected network, the behavior is analogous except that flow will occur only when the fluid yields to allow flow along a connected set of paths between the inlet and outlet, as shown previously in idealized networks (Sahimi, 1993; Shah et al., 1995). This phenomenon is observed in the current model by applying a fixed pressure gradient across the packed bed and solving for the pressure in each pore. At very low applied pressure gradients, the fluid yields nowhere because the pressure drops (across pore throats) do not generate sufficient internal stresses to overcome the yield stress. At somewhat larger pressure gradients, selected pore throats will be exposed to large-enough wall stresses to exceed the yield stress. However, if enough smaller throats remain closed at this pressure gradient, the net flow rate remains zero. (Note that this phenomenon cannot be observed when the rigorous Bingham constitutive equation is enforced, because the pressure is indeterminate. However, it is observed with the approximate constitutive equation for cases where ΔP_m is arbitrarily close ΔP^*.) Finally, when enough throats yield so as to form a connected path from one end of the network to the other, flow is observed.

In this work, we refer to the threshold pressure gradient as the lowest pressure gradient at which flow through the packed bed occurs. Figure 10 contains images of the network at three different pressure gradients, beginning at the threshold pressure gradient for the particular network/fluid combination that was used (see caption); the black indicates the conductive path(s) for fluid flow.

This critical behavior has important implications for miscible fluid displacement. Typically, one miscible fluid will displace another completely, given sufficient time. However, if the displaced fluid is a yield-stress fluid, and a fraction of pore

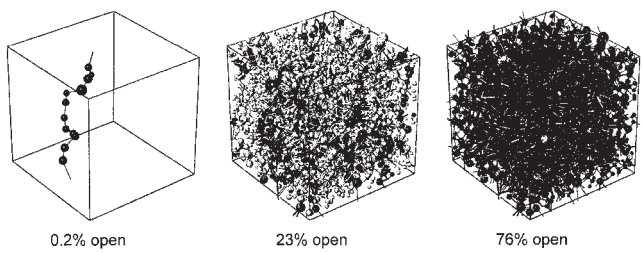

Figure 10. Qualitative results showing percolation paths in the network model for increasing pressure gradient.

The Figure shows % of bonds open to flow. The Bingham fluid modeled has rheological properties, $\tau_0 = 10$ Pa, $\mu_0 = 0.1$ Pa-s, and the specified bed had a uniform particle diameter of 0.2 cm and porosity of 38%. The measured permeability is 3.12×10^{-5} cm^2.

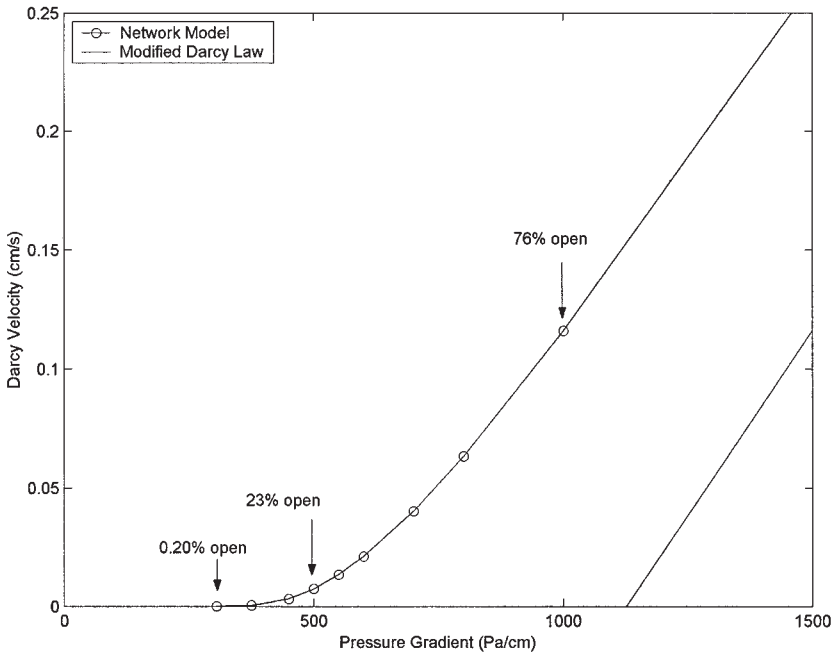

Figure 11. Quantitative results of Darcy velocity vs. pressure gradient comparing network model to the modified Darcy's law shown in Eq. 2.

Fluid and bed properties are the same as in Figure 10. The network permeability was substituted into Eq. 2 for comparison.

throats does not yield, then the displacement will be more analogous to an immiscible displacement, with a trapped phase remaining behind. This effect will be pronounced if the displaced phase has a higher bulk viscosity (for example, water displacing a highly viscous polymer gel), because the pressure gradient will decrease during the injection sequence (for constant rate displacement), which may cause additional pore throats to return to an unyielded state.

A note should be made regarding the solution at low-pressure gradients (below the threshold gradient). Numerical calculation of whether interior throats have yielded makes use of the pressure distribution obtained using one of the approximate equations for flow (see Figure 9). The implicit assumption is that the stress distribution in the unyielded material is similar to the stress distribution for flow. (The issue here is not with the approximate equations vs. the rigorous equations, but that we have made no *a-priori* statements about the stress-strain behavior of the unyielded material.) For a single tube, using the Newtonian pressure field is equivalent to assuming that the unyielded gel is an incompressible, linear elastic material constrained from slipping at the walls, which is not an unreasonable assumption. Extending this logic to the packed bed requires that the network-model approach be a valid way to approximate the stress propagation in the porous media, which is a more complex issue. While these considerations are important, they are not addressed further because the focus of this work is on flow at the threshold pressure gradient and above. We have shown that these solid-mechanics issues do not affect calculation of the threshold gradient by solving the rigorous Bingham equations (starting at higher pressure gradients and moving down), and then solving the approximate equations (starting at low-pressure gradients and moving up). These two approaches give the same percolation path and threshold gradient.

Quantitative description of flow

Using the Network model, quantitative relationships for Darcy velocity vs. pressure gradient can be developed. Figure 11 contains results for a particular fluid and packed-bed combination (rheological properties and morphologic properties are shown in the caption). Also plotted is the flow behavior predicted by the modified Darcy's law (Eq. 2) presented by Al-Fariss and Pinder (1987), using the same rheological and morphological properties.

Two major differences exist between the results from the network model, and those obtained from the modified Darcy's law. First, the semi-empirical model predicts the relationship to be linear for a Bingham fluid, with an x-intercept at the threshold gradient; whereas the network model predicts a nonlinear relationship at low-pressure gradients. Second, the predicted threshold gradient is significantly lower for the network model, (giving higher Darcy velocities for a given pressure gradient in the finite flow regime).

The network model predicts nonlinear behavior at low-pressure gradients for two reasons. First, Eq. 5 is nonlinear (with respect to pressure gradient) because the size of the unyielded core decreases with increasing flow. In contrast, the modified Darcy's law uses a simplified velocity profile and the nonlinear terms in the expression for flow are ignored. Second, the network model accounts for the natural heterogeneity in the packed bed. Throats in the network are of varying size, and, therefore, open sequentially with increasing pressure gradient, which leads to increased conductivity. Conversely, the modified Darcy's law assumes a bundle of uniform-sized tubes, and the yield point occurs everywhere at a single value of the applied pressure gradient. This latter effect (that is, heterogeneity) can be observed in Figure 10 images, which correspond to the three locations marked by arrows in Figure 11.

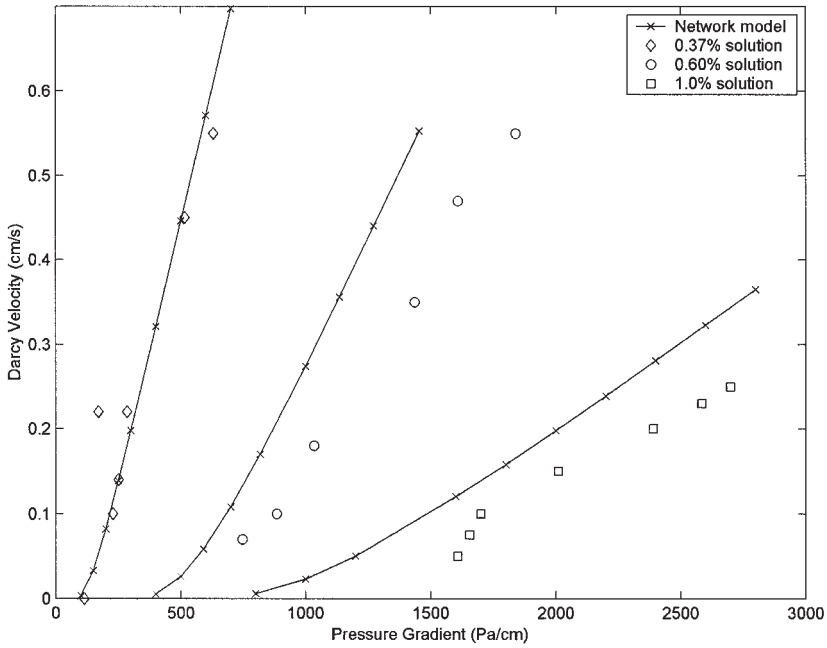

Figure 12. Darcy velocity vs. pressure gradient for the experimental work presented by Chase (2003).

The Bingham fluids used were aqueous solutions of Carbopol: (a) 0.37% solution with rheological parameters $\tau_0 = 2.2$ Pa and $\mu_0 = 0.025$ Pa-s; (b) 0.6% solution, $\tau_0 = 9.0$ Pa and $\mu_0 = 0.05$ Pa-s, and (c) 1.0% solution, $\tau_0 = 17.0$ Pa and $\mu_0 = 0.15$ Pa-s. The bed was packed with glass beads of particle diameter 0.211 cm at 37% porosity. Experimental data were estimated from plots in the referenced article.

The more significant observation from Figure 11 is that the network curve is shifted to the left of the modified Darcy's relationship. The curves are parallel at high pressure gradients with slope equal to K/μ_0, but the network model predicts a lower threshold gradient and a higher Darcy velocity at all pressure gradients. There are at least three fundamental reasons for the difference:

(1) *Parallel heterogeneity.* The bundle-of-tubes approach employed in the derivation of the modified Darcy's law assumes that each tube is the same size. Therefore, flow yields everywhere at exactly the same pressure gradient. In the network model, certain throats in the network will allow flow to occur before other throats will because of microscopic heterogeneity. Accordingly, the threshold pressure gradient corresponds to the path (in the context of a Bingham fluid) that is conductive at the lowest-pressure gradient to allow flow, which is lower than the pressure gradient that is predicted in an average sense. Sahimi (1993) has observed this same behavior when comparing Monte Carlo network simulations vs. effective medium theory for the case of transport with critical behavior.

(2) Series Heterogeneity. Each percolation path through a real porous medium contains series heterogeneities that are not captured by the bundle-of-tubes models. In these models an equivalent tube is created with uniform radius, and the same conductivity as the heterogeneous throats in series. However, the equivalent tube does not, in general, predict the same threshold gradient.

(3) Converging-diverging throat geometries. In the network model, we account for converging/diverging geometry, as described previously. In the modified Darcy's law, the surface area term comes from an estimate of the hydraulic radius along with the bed length (the latter adjusted for tortuosity), both of which are derived from semiempirical arguments for flow of Newtonian fluids. Since frictional losses during creeping flow of Newtonian fluids depend on total surface area, the bundle-of-tubes models are expected to overestimate the threshold pressure gradient.

Analysis of the model results

A limited amount of experimental data has been published for the flow of yield-stress fluids in packed beds (Park, 1971; Al-Fariss and Pinder, 1987; Chase and Dachavijit, 2003). In each case, a simple constitutive model (Bingham or Herschel-Bulkley) was assumed for the fluid, and rheological parameters (that is, μ_0, τ_0, n) were determined using a least-squares fit to the rheological data. Data were collected for the pressure gradient as a function of velocity in packed beds. Al-Fariss and Pinder (1987) and Chase and Dachavijit (2003) referred to a threshold gradient for flow initiation, but for constant flow rate experiments a threshold gradient can only be estimated through extrapolation to zero flow. This method is somewhat subjective since a no-flow condition is never truly observed.

Chase and Dachavijit (2003) used various concentrations of Carbopol 941 solution, and used a Bingham equation to model shear stress vs shear rate data. The model fit relatively well, although some systematic deviation was observed, particularly at low- shear rates. Using the measured rheological and bed properties, the network model was run and compared to the experimental data. Figure 12 shows quite good agreement between the experimental data and the network results, especially noting that the network-model results were obtained by direct substitution of the packed bed and rheological properties from the referenced article into the model, with no adjustable parameters. Chase and Dachavijit (2003) compared the exper-

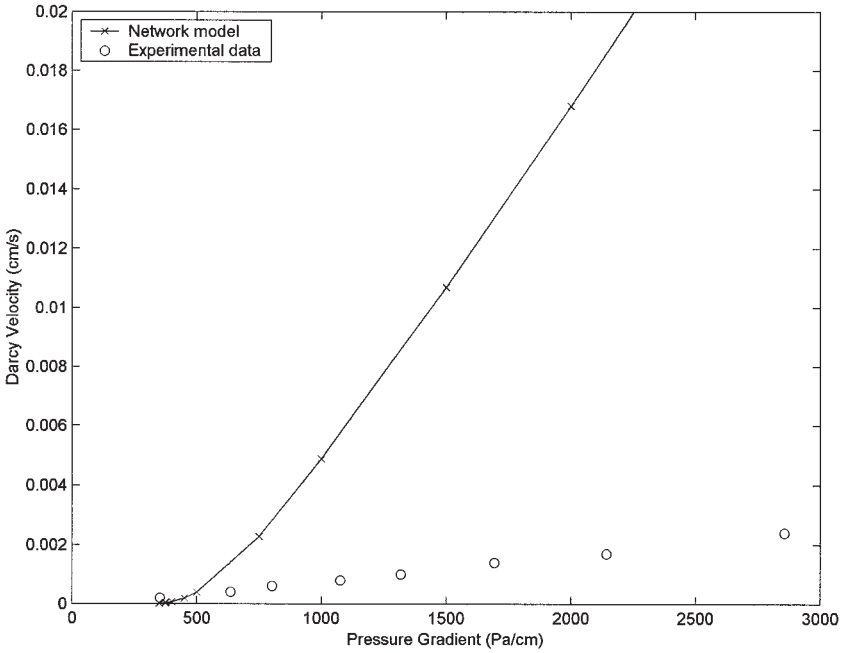

Figure 13. Darcy velocity vs. pressure gradient for the experimental work presented by Al-Fariss and Pinder (1987).

The Herschel-Bulkley fluid used was 2.5% Parvan 55 in Clarus B oil at 18°C with measured rheological parameters, $\tau_0 = 3.15$Pa, $\mu_0 = 0.335$ Pa-s, and $n = 0.97$. The bed was packed with glass beads of particle diameter 0.077 cm and 36% porosity.

imental results to their modified Ergun equation, and then added an experimental constant in the threshold gradient term to account for the assumptions of the bundle-of-tubes approach used in the derivation. Although the constant was determined from a wide range of concentrations of Carbopol solutions, it is not known whether the adjusted modified equation could be applied to other Bingham fluids and packed beds.

Al-Fariss and Pinder (1987) conducted flow tests using a Paraffinic wax (Parvan 55) in oil (Clarus-B or Clarus-C). Rheological tests of the fluid were conducted for a wide variety of concentrations and temperatures, and the data were fit to a Herschel-Bulkley model. Flow tests were performed in packed beds of sand ($D_p = 0.077$ cm, $\phi = 36\%$), for which a Newtonian permeability of 3.15×10^{-6} cm^2 was measured. To model flow of the non-Newtonian fluids, the authors adjusted the modified Darcy's law to fit their experimental data for each specific fluid/bed combination that was tested. The adjustments were made by obtaining a best fit, and then by altering the permeability, threshold gradient term, and power-law index in Eq. 2. Since these adjustments were made on an experiment-by-experiment basis, it is unlikely that they could be used for the prediction of Bingham-fluid flow in a general sense.

One of the fluids that exhibits nearly Bingham behavior ($n = 0.97$) was chosen to compare with the network model. An excellent fit to the rheological model is provided in Al-Fariss and Pinder (1987). The packed bed was modeled using uniform spheres (since no size distribution is provided in the referenced article). Mean sphere diameter and porosity were matched to the experimental values, and the permeability estimated by the network model (3.69×10^{-6} cm^2) compares favorably to the experimental results.

Figure 13 is a comparison of the experimental data to the results of the Network model, which shows rather poor agreement. Al-Farris and Pinder (1987) also note that the data match poorly to the modified Darcy's law (without any empirical adjustments). They argue that the reason for the discrepancy is that the effective permeability will be less for yield-stress fluids (than for fluids without a yield stress), because some pores in the bed will contain unyielded fluid and will, therefore, be blocked to flow. Our results show that the discrepancy cannot be attributed to this rheological effect because it is significant only at low-pressure gradients (see Figures 9 and 10), and at high-pressure gradients flow should approximate Newtonian behavior.

In Figure 13, the major difference between the experimental data and network model is not the value of the threshold gradient, but rather the Darcy velocity at high-pressure gradients, where the slope should be nearly equal to K/μ_0. This order-of-magnitude discrepancy in slope between the predicted and measured values must be attributed to either a reduction in the permeability of the porous medium or *in-situ* rheological behavior that differs significantly from what is observed in bulk measurements. Permeability reduction in porous media caused by non-Newtonian flow is not uncommon, and is reported in the literature (for example, Savins, 1969); absorption and filtration are examples of physical effects that can contribute to this effect. It is worth noting that network modeling, being a pore-scale approach, is an effective method to examine these phenomena, although more conclusive experimental evidence should be obtained before adopting this modeling strategy.

Park (1971) used aqueous solutions of polymethylcellulose (PMC) to conduct experimental tests of flow in packed beds. Rheological data were obtained at two concentrations and two molecular weights of PMC. A Herschel-Bulkley model fit the data with acceptable accuracy. However, due to the strong shear-thinning behavior of the fluid ($n = 0.57$), these data

could not be compared quantitatively to the current model, without developing an appropriate set of flow rate equations (analogous to Eq. 5) for Herschel-Bulkley fluids.

Conclusions

The flow of non-Newtonian fluids in packed beds is important in many practical applications, and equations and theory for yield-stress fluids is unique, because a threshold pressure gradient is required to initiate flow. A number of macroscopic relationships, which are used for continuum-scale modeling have been proposed for non-Newtonian fluids and a few are applicable for yield-stress fluids. While these simple, closed-form expressions are convenient when applicable, they are also quite restrictive in how they are applied.

Network models have been used extensively to understand fundamental aspects of flow in porous media. In this work, we used computer-generated sphere-packings to construct physically representative models of packed beds, which in turn allows for the quantitative modeling of flow. An algorithm is described for modeling the steady flow of a Bingham fluid in the packed bed. It is also applicable to other non-Newtonian fluids, although certain critical network parameters have been evaluated only for the Bingham case.

Modeling of this highly nonlinear process illustrates the importance of retaining proper pore morphology into the physically representative network models. Specifically, linear problems require only the hydraulic conductivity of pore throats to be known; however, additional parameters are required for nonlinear flows, which are rarely considered when generating the capillary networks commonly used in network modeling. The approach proposed here is to avoid transforming the network into capillaries at the initial stage, and, instead, to construct the network using rigorous geometric parameters. If later transformation into simple geometries is required (to accommodate flow modeling), it should be performed on a case-by-case basis, depending on the physics of the flow.

Comparison of the model with experimental data from Chase and Dachavijit (2003) shows good agreement, suggesting that the model captures quantitative flow behavior. The comparison with data from Al-Fariss and Pinder (1987) is much poorer. Qualitative arguments suggest that the discrepancy is a result of permeability reduction (possibly caused by filtration or absorption), or a fluid rheology that is inconsistent with the reported measured rheological parameters, rather than a problem with the network model.

Finally, we note that the network model possesses important attributes not found in simpler capillary models. First, it provides context for interpreting empirical corrections that are commonly applied to the capillary models. (In the current study, it shows that empirical corrections applied to the modified Darcy's law are not attributed to factors, such as tortuosity, interconnectivity, or heterogeneity.) Second, key parameters, such as particle-size distribution or packing heterogeneity, can be incorporated into the model explicitly. Finally, the network model can be readily extended for the modeling of transient processes (for example, displacement of the yield-stress fluid from the packing).

Acknowledgments

This work was funded by NSF/IGERT grant No. 9987603, and by Schlumberger Technology Corporation. The authors would like to thank Schlumberger for additional in-kind support, Jean Desroches, Eddie Siebrits, Matthew Miller, and Joseph Ayoub for valuable discussions and suggestions, and Prof. Erik Thompson for aid with the FEM simulations. Computations were performed using CaSPer, which is part of LSU's high-performance computing network.

Notation

a = geometric parameter for general duct
C = tortuosity constant
D_p = particle diameter
g = hydraulic conductivity
K = permeability
L = tube length
$LYPR$ = linear yield point ratio
n = power-law index
P = pressure
ΔP = pressure drop across duct/tube
ΔP^* = critical pressure drop required to initiate flow
ΔP^*_{lin} = linear critical pressure drop
ΔP_D = dimensionless pressure drop
ΔP_m = pressure drop that approximate curve equals actual curve
q = throat flow rate
R = tube radius
S = surface area
S_{eff} = effective surface area
v = velocity
v_0 = Darcy velocity
YPR = yield point ratio

Greek letters

γ_R = aspect ratio
τ = shear stress
τ_w = wall stress
τ_0 = yield stress
μ = viscosity
μ_{eff} = effective viscosity
μ_0 = viscosity constant in Herschel-Bulkley model

Subscripts

cap = cylindrical capillary tube
$duct$ = arbitrary duct
i = pore
j = adjacent pore

Literature Cited

Al-Fariss T, and K. L. Pinder, "Flow of a Shear-Thinning Liquid with a Yield Stress Through a Porous Media," *SPE 13840, Society of Petroleum Engineers* (1985).

Al-Fariss T, and K. L. Pinder, "Flow Through Porous Media of a Shear-Thinning Liquid with a Yield Stress," *Can. J. Chem. Eng*., **69**(3), 391 (1987).

Al-Raoush, R., K. E.Thompson, and C. S. Willson, "Comparison of Network Generation Techniques for Unconsolidated Porous Media," *SSSA J*. **67**, 1687 (2003).

Bakke, S., and P. E. Oren, "3-D Pore-Scale Modelling of Sandstones and Flow Simulations in the Pore Networks," *SPE J*., **2**(2), 136 (1997).

Beverly, C. R., and R. I. Tanner, "Numerical Analysis of Three-Dimensional Bingham Plastic Flow," *J. of Non-Newtonian Fluid Mech.*, **42**, 85 (1992).

Bird, R. B., R. C. Armstrong, and O. Hassager, *Dynamics of Polymeric Liquids,* 2nd ed., Wiley, New York (1987).

Bird, R. B., W. E. Stewart, and E. N. Lightfoot, *Transport Phenomena*, 2nd ed., Wiley, New York (2002).

Bryant, S. L., D. W. Mellor, and C. A. Cade, "Physically Representative Network Models of Transport in Porous Media," *AIChE J*., **39**, 387 (1993).

Carreau, P. J, D. C. R. De Kee, and R. P. Chhabra, *Rheology of Polymeric Systems*, Hanser/Gardner, Cincinatti, OH (1997).

Carman, P. C., "Permeability of Saturated Sands, Soils and Clays," *J. Agr. Sci*., **29**, 262 (1939).
Chase, G. G., and P. Dachavijit, "Incompressible Cake Filtration of a Yield Stress Fluid," *Sep. Sci. Tech*., **38**(4), 745 (2003).
Dillard, L. A., and M. J. Blunt, "Development of a Pore Network Simulation Model to Study Nonaqueous Phase Liquid Dissolution," *Water Resour. Res*., **36**, 439 (2000).
Jensen, J. L., L. W. Lake, P. W. M. Corbett, and D. J. Goggin, *Statistics for Petroleum Engineers and Geoscientists*, Prentice Hall PTR, Upper Saddle River, NJ (1997).
Jodrey, W. S., and E. M. Tory, "Computer Simulation of Close Random Packing of Equal Spheres," *Phys. Rev. A*., **32**(4), 2347 (1985).
Lenormand, R., E. Touboul, and C. Zarcone, "Numerical Models and Experiments on Immiscible Displacements in Porous Media," *J. Fluid Mech.,* **189,** 165 (1988).
Lopez, X., P. H. Valvatne, and M. J. Blunt, "Predictive Network Modeling of Single-Phase non-Newtonian Flow in Porous Media," *J. Colloid Interface Sci.,* **264**(1), 256 (2003).
Mellor, D. W., "Random Close Packing (RCP) of Equal Spheres: Structure and Implications for Use as a Model Porous Medium," PhD Thesis, Open University, Milton Keynes, U.K. (1989).
Park, H. C., "The Flow of Non-Newtonian Fluids through Porous Media," PhD Thesis, Dept. of Chemical Engineering, Michigan State University (1972).
Pascal, H., "Non-Steady Flow through Porous Media in the Presence of a Threshold Gradient," *Acta Mech*., **39**(3-4), 207 (1981).
Patzek, T. W., "Verification of a Complete Pore Network Simulator of Drainage and Imbibition," *SPE J*., **6**(2), 144 (2001).
Powell, M. J., "Computer-Simulated Random Packing of Spheres," *Powder Technol.*, **25**, 45 (1980).
Press, W. H., S. A. Teukolsky., W. T. Vetterling, and B. P. Flannery, *Numerical Recipes in Fortran 77*, 2nd ed., Cambridge University Press, New York (1992).
Sahimi, M., "Nonlinear Transport Processes in Disordered Media," *AIChE J*., **39**(3), 369 (1993).
Sahimi, M., A. O. Imdakm, 'The Effect of Morphological Disorder on Hydrodynamic Dispersion in Flow Through Porous Media," *J. Phys. A: Math. Gen.,* **21**, 3833 (1988).
Satyadev, C. N., K. Jayaraman, C. A. Petty, N. S. Losure, "Stability of Polymerizing Liquid Flow in Porous Media," *Polym. React. Eng.,* **8**(2),167 (2000).
Savins, J. G., "Non-Newtonian Flow through Porous Media," *Ind. Eng. Chem.,* **61**(10), 18 (1969).
Shah, C. B, H. Kharabaf, and Y. C. Yortsos, "Flow and Displacement of Bingham Plastics in Porous Media," presented at *Proc. Unitar Conf. On Heavy Oils and Tar Sands*, Houston, TX (Feb. 16, 1995).
Shah, C. B., H. Kharabaf, and Y. C. Yortsos, "Immiscible Displacements Involving Power-Law Fluids in Porous Media," presented at *Proc. Unitar Conf. On Heavy Oils and Tar Sands*, Beijing, China (Oct. 27, 1998).
Shah, C. B., and Y. C. Yortsos, "Aspects of Flow of Power-Law Fluids in Porous Media," *AIChE J*., **41**, 1099 (1995).
Sisavath, S., X. Jing, C. C. Pain, and R.W. Zimmerman, "Creeping Flow Through an Axisymmetric Sudden Contraction or Expansion," *J. Fluids Eng.*, **124**, 273 (2002).
Sisavath, S., X. Jing, and R. W. Zimmerman, "Laminar Flow Through Irregularly-Shaped Pores in Sedimentary Rocks," *Trans. Porous Media*, **45**(1), 41(2001).
Skartsis, L. B., B. Khomami, and J. L. Kardos,"Semi-Analytical One-Dimensional Model for Viscoelastic Impregnation of Fibrous Media," *J. Adv. Materials*., **25**, 38 (1994).
Skelland, A. H. P., *Non-Newtonian Flow and Heat Transfer*, Wiley, New York (1967).
Sorbie, K. S., P. J Clifford, and E. R. W. Jones, "The Rheology of Pseudoplastic Fluids in Porous Media Using Network Modeling," *J. Colloid Interf. Sci.*, **130**, 508 (1989).
Thauvin, F., and K. K. Mohanty, "Network Modeling of Non-Darcy Flow Through Porous Media," *Trans. Porous Media*, **31**(1), 19 (1998).
Thompson, K. E., and H. S. Fogler, "Modeling Flow in Disordered Packed Beds from Pore-Scale Fluid Mechanics," *AIChE J*., **43**, 1377 (1997).
Thompson, K. E., "Pore-Scale Modeling of Fluid Transport in Disordered Fibrous Materials," *AIChE J.*, **48**(7), 1369 (2002).
Vogel, H. J, and K. Roth, "Quantitative Morphology and Network Representation of Soil Pore Structure," *Adv. Water Resour.,* **24**(3-4), 233 (2001).
Vradis G. C., and A. L. Protopapas, "Macroscopic Conductivities for Flow of Bingham Plastics in Porous Media," *HY*., **119**(1), 95 (1993).

Appendix A

Streamline-Scale Modeling

For Newtonian fluid flow in a duct, the flow rate vs. pressure drop relationship is linear at low-Reynolds numbers, regardless of the duct geometry. Hence, even for complex-shaped ducts, this relationship can be captured by a single scalar hydraulic conductivity term. For non-Newtonian fluids, additional geometric term(s) can appear in the expression for flow rate. For instance, as shown by Eqs. 5 and 7, flow of a Bingham fluid in a cylindrical duct contains the hydraulic conductivity, as well as the duct surface area.

In either case, numerical modeling of microscale flow can be used to help estimate throat hydraulic conductivities g_{ij}. For the Newtonian case, this approach is valuable because of the complex geometries encountered in the network (Thompson and Fogler, 1997). However, simpler approaches can also be used, which make use of known functionalities between frictional loss and duct geometries (for example, Sisavath et al., 2001, 2002). In this article, due to the non-Newtonian behavior, detailed simulations have been used, because it is not clear how to properly choose the equivalent throat geometries so as to quantify the flow behavior.

To characterize yield-stress flows in converging-diverging ducts, finite-element-method (FEM) simulations were performed using idealized, axisymmetric geometries. The equations of motion for creeping flow were solved using a Galerkin FEM formulation. The fluid rheology was for a Bingham fluid, which was modeled using an approximate constitutive equation (Beverly and Tanner, 1992). No-slip boundary conditions were imposed along the surfaces of the duct. At the inlet and outlet, the normal component of stress was specified, and tangential velocity was set equal to zero. These inlet/outlet boundary conditions are valid for a duct having symmetry reflected across the r-θ plane. Although this symmetry is certainly not present in pore-throats of the packed bed, the approximations made here (and the empiricism described in the body of the article) are commensurate with general assumptions made in network modeling.

Flow was modeled for a variety of axisymmetric, converging-diverging geometries. Figure 5 illustrates the flow patterns in a duct with a circular constriction rotated around the axis of symmetry (which coincides with the bottom of the figure). Other constriction shapes included ellipses (with their long axes oriented both horizontally and vertically), squares, and trapezoids. The flow domains were meshed using Delaunay triangulation. Six-node triangles were used for velocities, and pressure was assumed constant over each element. A mixed method formulation was used. Local mesh refinement was performed in areas of high stresses to ensure reasonable accuracy.

Manuscript received Oct. 23, 2003, and revision received Apr. 6, 2004.